We are IntechOpen, the world's leading publisher of Open Access books Built by scientists, for scientists

6,900
Open access books available

186,000
International authors and editors

200M
Downloads

Our authors are among the

154
Countries delivered to

TOP 1%
most cited scientists

12.2%
Contributors from top 500 universities

WEB OF SCIENCE™

Selection of our books indexed in the Book Citation Index in Web of Science™ Core Collection (BKCI)

Interested in publishing with us?
Contact book.department@intechopen.com

Numbers displayed above are based on latest data collected.
For more information visit www.intechopen.com

20

On the Use of ACO Algorithm for Electromagnetic Designs

Eva Rajo-Iglesias, Óscar Quevedo-Teruel and Luis Inclán-Sánchez
University Carlos III of Madrid
Spain

1. Introduction

The use of Global Search Optimization Methods to solve electromagnetic problems has been widely extended. Among these methods the most popular ones for the antenna and electromagnetism communities are Genetic Algorithms (GA) and recently Particle Swarm Optimization (PSO). Algorithms based on these methods have been used to face the design of arrays and other types of antennas (Ares-Pena et al. (1999); Yan & Lu (1997); Tennant et al. (1994); Robinson & Rahmat-Samii (2004); Khodier & Christodoulou (2005)). It is always a matter of discussion which algorithm to use for a given problem, being this topic considered as an *art* as discussed in (Quevedo-Teruel et al. (2007)). In this sense we propose in this chapter the application of an algorithm based on ACO (using real numbers) to solve several electromagnetic problems. The algorithm is implemented in such a way that fits well to problems where the desired solution is not far away from the initial one but where the evaluation of solutions is time demanding.

2. Algorithm description

The Ant Colony Optimization was developed by Dorigo in 1996 (Dorigo et al. (1996), Dorigo et al. (1999), Dorigo & Stutzle (2004)) and it has been used to solve a different type of problems (Hoshyar et al. (2000), Wang et al. (2005), Bullnheimer et al. (1999)) by employing different realizations of the algorithm. The usefulness of this optimization technique is especially powerful in distributed problems like (Sim & Sun (2003), Ahuja & Pahwa (2005), Premprayoon & Wardkein (2005)) and (Liang & Smith (2004)). This algorithm is based on the behavior of ant colonies when they are looking for food and storing it in their nests.
ACO has been very rarely used to solve electromagnetic problems (Coleman et al. (2004), Quevedo-Teruel & Rajo-Iglesias (2006), Rajo-Iglesias & Quevedo-Teruel (2007)), however its characteristics could be interesting for this purpose in some situations as it will be shown along this chapter.

2.1 Basis of the algorithm

For many authors, Ant Colony Optimization is a particular case of PSO, since biologically a colony of ants is a particular case of swarm (Dorigo et al. (2004)), however ACO uses some bases of operation that makes it clearly different from PSO. ACO means algorithms based on the ant behavior in the searching for food and posterior transportation to the nest to be stored. These insects have the ability of finding the "shortest path" in this task by using pheromones.

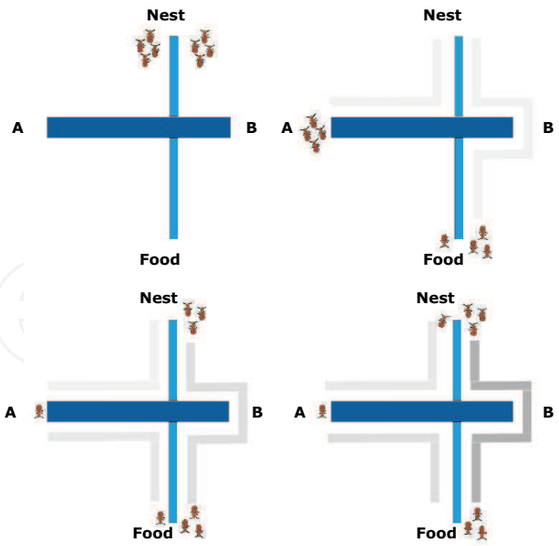

Fig. 1. Diagram of pheromone operation in Ant Colony

Some ant species use pheromones for making paths on the ground, in their way from food to the nest. This helps other ants, by pheromones sensing, to follow the path towards food discovered by other ants. Because ants deposit pheromones while walking, a larger number of ants on a path results in a larger amount of pheromones, this larger amount of pheromones stimulates more ants to choose that path and so on until the ants finally converge to one single (short) path. These pheromones also evaporate with time to "delete" the path to an exhausted food source.

Figure 1 shows a graphical example of ant behavior. The ant nest, a food source and two possible paths are depicted. These two paths are of unequal lengths, and it is assumed that the longest path (path A) takes two time steps to cover, whilst the shortest one (path B) takes only a single time step. At $t = 0$, eight ants are introduced into the system with the objective of getting food and bringing it back to the nest. The initial selection of the path is random, then it is assumed that four ants select each one of the two possible paths. At $t = 1$, the ants that have chosen the shortest path B have acquired the food and begin to travel back home. As there is existing pheromone on path B the ants have a higher probability of using this path, consequently three ants select path B and one ant selects path A. The ants that had chosen path A are only half way along this path. At $t = 2$, the three ants that traversed path B are at home again whilst the ant that embarked on path A only half way along this path. The four ants that were traversing A have made it to food and embark on their journey back home via either path A or B. Path B has a larger amount of pheromone on it (the pheromone intensity is represented by the darkness of the path) as it has been traversed seven times, whereas path A has only been traversed five times. Consequently, by probability, three ants select path B and one ant selects A.

Finally, at $t = 3$, three ants have returned to the nest along path B except the one that is still in the middle of path A, being also three more ants that decided to take path B, and they have found the food. At that time, path B has a greater amount of pheromone on it as it has been traversed thirteen times in total, while the longer path A has been traversed only five times. Future ants entering the system will have a higher probability of selecting path

B. The diagram in Figure 1 illustrated how the swarm intelligence operates to determine the shortest path. The pheromone trails also decay with time. This means that in paths that are not regularly used, pheromone concentration will eventually decay to zero intensity. This decaying quality of pheromone also helps in the ability of the Ant Colony to find the shorter paths. The longer paths, which receive less pheromone, will decay more rapidly enabling shorter paths to have a higher probability of being selected.
Although most of the ant population use paths with high pheromone concentration, there is always some ant exploring new paths. This avoids the algorithm stagnation. Further details of the implementation of this algorithm will be discussed in Section 3.1.

3. Examples

We will present along this chapter some of the examples which show how useful this algorithm can be for electromagnetic designs.

3.1 Implementation of the Algorithm

In our implementation of the algorithm, an ant means a solution of the problem, and the main steps are the ones shown in the flowchart of Figure 2. Besides, we have to point out that there are two main states of operation, in the first one ($forward$) the ant is looking for food whilst in the second one (*backward*) the ant has to look for the path to come back home.
Paths are divided into nodes and, to decide the next node the ant is going to move towards, typically, the most extended decision criterium is the one proposed by Dorigo et al. (1996) and described as:

$$p_{i,j}(t) = \frac{[\tau_j(t)]^\alpha \cdot [\eta_j]^\beta}{\sum_{l \in \theta_i} [\tau_l(t)]^\alpha \cdot [\eta_l]^\beta} \tag{1}$$

Where $p_{i,j}$ is the probability of node j to be chosen at iteration t being at node i, $\tau_j(t)$ represents the pheromone concentration associated with node j at iteration t, α establishes the importance of pheromone concentration in the decision process whilst β does the same with the desirability, η_j is the desirability of node j, and θ_i is the set of nodes l available at decision point i.
The desirability η_j is a function that depends on the optimization goal. This function has to be evaluated at every node j for every ant. Its role is equivalent to the one of the fitness function in other algorithms. When the algorithm is developed, the definition of this function is one of the critical issues, as in many other algorithms.
The function τ_j can be implemented in different ways. In our case, we will use the expression:

$$\tau_j(t+1) = \tau_j(t) + \Delta\tau_j(t) - d(t) \tag{2}$$

Where $\Delta\tau_j(t)$ is the pheromone addition on node j, and $d(t)$ is the pheromone persistence:

$$d(t) = \begin{cases} \rho & \text{if } \mathrm{mod}\left(\frac{t}{\gamma}\right) = 0 \\ 0 & \text{if } \mathrm{mod}\left(\frac{t}{\gamma}\right) \neq 0 \end{cases} \tag{3}$$

Where γ is the period of pheromone elimination, and ρ is the coefficient of pheromone elimination by period.
The choice of the values of γ and ρ parameters is critical to achieve good results. For the particular examples that will be studied along the following pages, these values have been empirically selected as $\gamma = 20$, $\rho = 1$. The pheromone addition has been defined as $\Delta\tau_{i,j}(t) = 1$

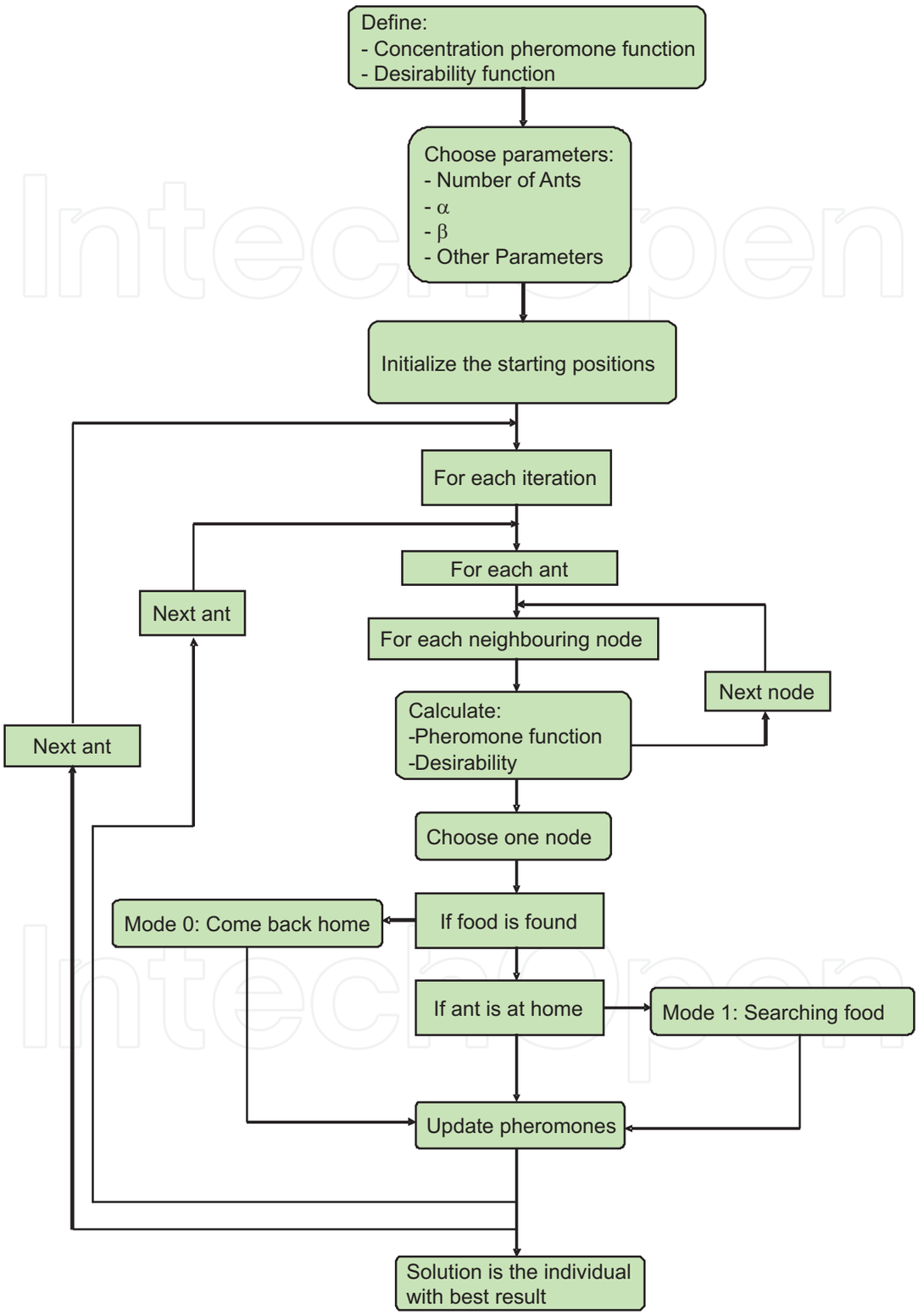

Fig. 2. Flowchart of the principal steps in the proposed Ant Algorithm

when an ant goes to the node j from any node i. On the other hand, the parameters α and β have been set differently for each example depending on the optimization goal.
Obviously, the value of $\Delta\tau_{i,j}(t)$ and the parameters γ and ρ are related to α, because they give the magnitude of the element $(\tau_j(t))$ that is raised to the power of α (Equations 1, 2 and 3).
As β is related to the importance of the desirability in the decision process whilst α does the same but with the pheromone concentration effect, for every example β has been chosen much larger than α in order to increase the effect of the better solutions on the pheromone concentration (that would fix strict ant trails and therefore, slow evolution of the algorithm or even, algorithm stagnation). The empirical selection of these parameters is a common issue in most optimization algorithms. However, some guidelines can be found in the theoretical basis of this method as well as some range of variation of the parameters (Dorigo & Stutzle (2004)).
The number of ants and/or iterations in the algorithm can be decided based on the computational capacity. The food is defined as the desired condition, i.e, for example in array synthesis, can be the Side Lobe Level (SLL), the null in given directions or a specific Beam Width (BW).

3.2 Array synthesis

The initial example of application of the algorithm is considered as a "classical" problem of optimization among the electromagnetic community. We are talking about the *array synthesis* where many other algorithms have been previously applied (Haupt & Werner (2007), Khodier & Christodoulou (2005),Robinson & Rahmat-Samii (2004)). Along this section we will show some examples of synthesis carried out by using an ACO algorithm (Quevedo-Teruel & Rajo-Iglesias (2006), Rajo-Iglesias & Quevedo-Teruel (2007)).

3.2.1 Linear array synthesis

We initially propose to deal with a simple case of synthesis: a linear array of $2N$ elements, all of them with uniform amplitude and phase. The optimization will be performed changing the element positions (becoming a non-equally spaced array, but keeping symmetry) as in (Khodier & Christodoulou (2005), Jin & Rahmat-Samii (2007)).
The initial array is composed of $2N$ elements uniformly distributed along the $\hat{z}$ axis. The Array Factor (AF) in this case can be written as

$$AF(\theta) = 2\sum_{n=1}^{N} I_n cos[k \cdot z_n \cdot \cos(\theta) + \varphi_n] \tag{4}$$

If the amplitude and phase are uniform ($I_n = I_0, \phi_n = \phi_0$), the AF can be simplified as

$$AF(\theta) = 2\sum_{n=1}^{N} cos[k \cdot z_n \cdot \cos(\theta)] \tag{5}$$

Our goal will be to find out the positions $\{z_1, z_2, ..., z_N\}$ of the elements that accomplish the design requirements using an algorithm based on Ant Colony Optimization.
This example of synthesis is directly based on the work presented in (Khodier & Christodoulou (2005)) where Particle Swarm was used for this type of array synthesis. Here, we will present similar examples to the ones included in that paper.
ACO is discrete in nature, hence, a discretization of the variables that we use in the optimization process is needed. Consequently, the positions of the array elements will be

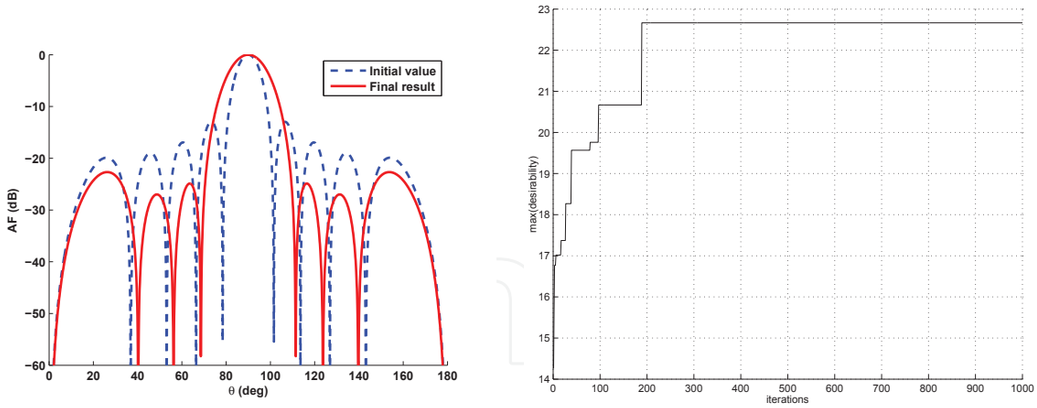

(a) Radiation pattern (b) Convergence

Fig. 3. Normalized radiation pattern of *10*-element linear array obtained by the ant algorithm (solid line) compared to the initial value (dotted line) and convergence of the algorithm

.

discretized. A step of 0.1λ has been considered in all the examples. In addition, the initial array element positions (*home*) have been chosen as the ones with an inter-element separation of 0.5λ. Moreover, when the ants have found the food, they have to come back to *home*, i.e. to these initial positions.

Next, we will show three particular examples having each one different design criteria: to minimize the SLL level, obtaining three null directions, and to minimize the SLL keeping the BW narrow and obtaining a null in a given direction. In all cases, the algorithm convergence as well as the defined desirability function will be shown. The values of α and β are respectively 1 and 5 for all the following cases.

A: SLL level

As a first example, the typical case of SLL minimization will be synthesized. The desirability will be defined as the absolute value of the SLL including all directions (in dB and normalized). This can be written as

$$\eta_j = |SLL|_{dB} \tag{6}$$

Figure 3 shows the achieved result after 1000 iterations when 20 ants are used, for the synthesis of a 10 element array. The food is defined as a SLL of -20 dB level. In the same Figure, the initial AF (with equally spaced elements) is plotted. The achieved solution has a SLL of -22.66 dB.

Figure 3.b includes a representation of the algorithm convergence. The plotted line corresponds to the node with best desirability found in every iteration. The algorithm converges in approximately 200 iterations.

The obtained solution (the one illustrated in Figure 3) has the following element positions:

$z_1 = 0.15\lambda$	$z_2 = 0.35\lambda$	$z_3 = 0.75\lambda$	$z_4 = 0.95\lambda$	$z_5 = 1.55\lambda$

B: three null directions

The second example is an array synthesis with three desired null directions in the radiation pattern (θ_1, θ_2 and θ_3). Actually, the three directions will be spatially closed in order to produce a null in an angular range. The definition of desirability function is especially critical in this case. Empirically it has been chosen the following

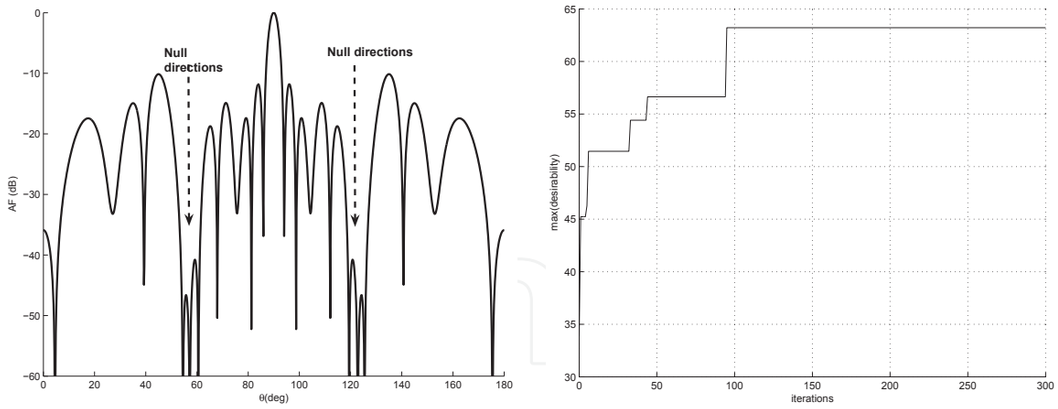

(a) Radiation pattern (b) Convergence

Fig. 4. Normalized radiation pattern of *28*-element linear array obtained by the ant algorithm and its convergence. Getting the three null directions at $\{55°, 57.5°, 60°\}$ and $\{120°, 122.5°, 125°\}$

$$\eta_j = \sqrt[3]{(|FA(\theta_1)|_{dB}) \cdot (|FA(\theta_2)|_{dB}) \cdot (|FA(\theta_3)|_{dB})} \tag{7}$$

Figure 4 shows an example of synthesis using 20 ants and 300 iterations. The number of array elements has been chosen to be 28 (N=14) and we have considered food when the normalized AF in directions $\{55°, 57.5°, 60°\}$ is -60 dB. Obviously, in the symmetrical directions $\{120°, 122.5°, 125°\}$ we have nulls too. The algorithm converges very fast, in approximately 100 iterations.
In this case, the solution for the array geometry is

z_1=0.15λ	z_2=0.55λ	z_3=1.25λ	z_4=1.65λ	z_5=2.75λ
z_6=2.95λ	z_7=3.25λ	z_8=3.75λ	z_9=4.15λ	z_{10}=4.45λ
z_{11}=5.15λ	z_{12}=5.75λ	z_{13}=5.85λ	z_{14}=6.65λ	

This array accomplishes with the required null radiation in the three directions as Figure 4 shows.

3.2.1.1 C: SLL, BW and null in a given direction

As a last example, three conditions will be imposed concerning SLL, BW and a null in a defined direction. Particularly a null will be required at θ=81°, a SLL below -15 dB and a BW of 7.7°. The array will have 32 elements.
To this aim 20 ants and 500 iterations have been used. As previously, the desirability function has to be carefully selected including now two modulating parameters $\beta_2 = 20$ and $\beta_3 = 6$. This can be expressed as

$$\eta_j = |FA(\theta_1)|^{\frac{1}{\beta_3}} \left(\frac{1}{BW(°) - \theta_f}\right)^{\frac{1}{\beta_2}} \cdot |SLL|_{dB} \tag{8}$$

A $\theta_f = 7°$ was used due to the minimum value of BW (with equally spaced elements) of 7.2°. After using this desirability function, the algorithm finds a solution that fulfills the required conditions. In this case, the array has a BW of 7.66° and a SLL of -17.85 dB, as well as the null

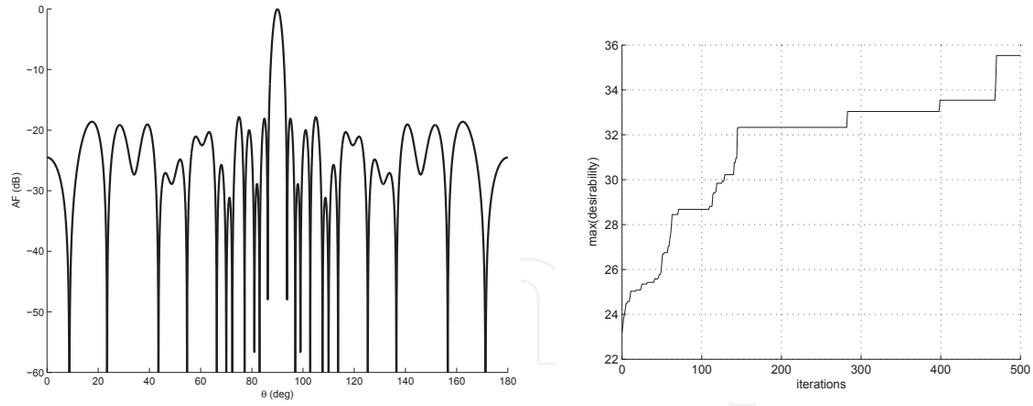

(a) Radiation pattern (b) Convergence

Fig. 5. Normalized radiation pattern and convergence of *32*-element linear array obtained by the ant algorithm. ($SLL < -15$dB, $BW < 7.7^\circ$, and a null at 81°)

in the specified direction (see Figure 5). A zoom of the central area is illustrated in Figure 6 in order to show the performances with detail.
The array with these characteristics has the elements distributed as follows,

z_1=0.35λ	z_2=0.65λ	z_3=1.15λ	z_4=1.55λ	z_5=2.15λ	z_6=2.75λ
z_7=3.15λ	z_8=3.25λ	z_9=3.85λ	z_{10}=4.35λ	z_{11}=4.85λ	z_{12}=5.45λ
z_{13}=6.25λ	z_{14}=7.05λ	z_{15}=7.65λ	z_{16}=8.35λ		

3.2.2 Thinned array

A second set of examples is devoted to synthesize thinned arrays which is another method of designing aperiodic arrays especially when the number of array elements is large (Schwartzman (1967), Haupt (1994), Haupt (2005)). We will now employ this method with the ACO algorithm, where the positions of the elements will be fixed but each element is able

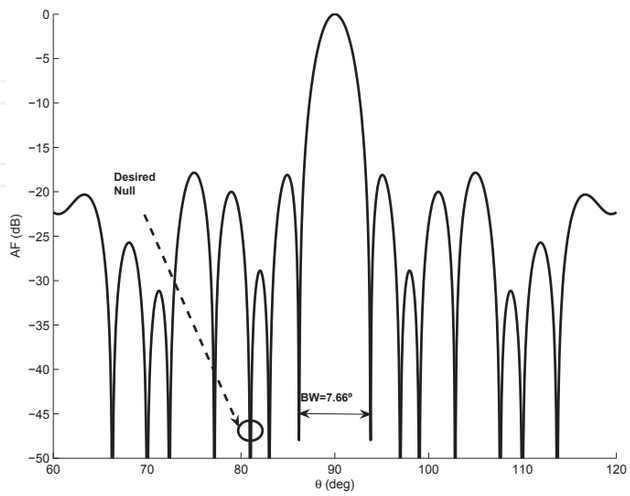

Fig. 6. Detail of the AF shown in Figure 5.a

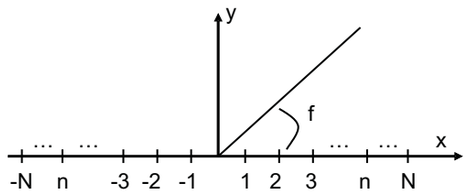

Fig. 7. Geometry of a $2N$-element symmetric linear array along x-axis

to present two states: "on" (when the element is fed) and "off" (when the element is passively terminated by an impedance equal to the source impedance of the fed elements).
According to the structure shown in Figure 7, where there are $2N$ elements symmetrically distributed along the x-axis, the array factor in the azimuth plane (XY plane) can be written as

$$AF(\phi) = 2\sum_{n=1}^{N} I_n cos[\frac{\pi}{2} \cdot (2n-1) \cdot \cos(\phi)] \tag{9}$$

where I_n is the excitation amplitude of the n^{th} element. In our case, I_n is 0 if the state of the n^{th} element is "off" and 1 if it is "on". The distance between elements is 0.5λ and all of them have identical phases.
Figure 8 shows a planar array structure of $2N \times 2M$ elements. The array factor for this structure is given by (assuming the same considerations as in the linear array case):

$$AF(\theta,\phi) = 4\sum_{n=1}^{N}\sum_{m=1}^{M} I_{nm} cos[\pi \cdot (2n-1) \cdot \sin(\theta)\cos(\phi)] \cdot cos[\pi \cdot (2m-1) \cdot \sin(\theta)\sin(\phi)] \tag{10}$$

Therefore, we need to find out which array elements should be enabled or disabled ($I_{nm} = 1$ or $I_{nm} = 0$) to get the desired radiation pattern characteristics.
For the thinned array optimization we will have N bits, thus corresponding to an N-dimensional space of solutions. In this case, every ant means an array solution, i.e., a vector with N bits. Ants describe paths that are divided into nodes. They move from one node to another through the N-dimensional space of solutions by checking the desirability and the pheromone concentration level of their neighboring nodes before making a probabilistic decision among all of them. A neighboring node is calculated by toggling the state of only one element of the array. This means that every ant has N neighboring nodes and has to decide which one among them to move towards, in a probabilistic manner.

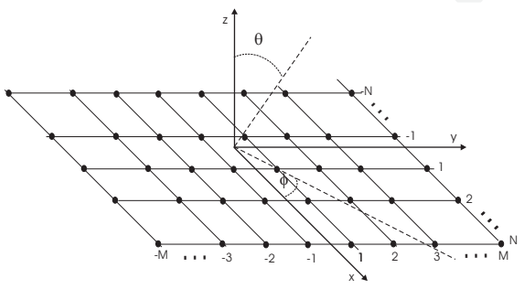

Fig. 8. Geometry of a $2N \times 2M$-element symmetric planar array in XY plane

We present now several examples to show how our ACO based algorithm performs in thinned array synthesis. In all the examples, we use as initial value the array with all elements "on" to take advantage of the entire structure that can be used.
In all the following examples we have set the parameter values as: $\alpha = 5$ and $\beta = 30$. The food is defined as a particular SLL value which changes depending on the example. However as our stopping criterion is to complete a number of iterations, the algorithm assigns better desirability values to solutions with lower SLL. Thus, even if the food is found, better solutions can be achieved and this often happens in the way back to the nest.

3.2.2.1 Linear array with a specific SLL

In this first example we search the lowest value of SLL with isotropic elements. The desirability is defined as the absolute value of the normalized SLL (in dBs).

$$\eta_j = |SLL(dB)| \tag{11}$$

Figures 9 and 10 show the result obtained with 10 ants, 100 iterations and 100 elements. Food was defined as -20 dB of SLL. In the same figure the initial case where all the elements were "on" has been plotted. The synthesized array accomplish the design goal. Besides we can see how the algorithm converges in approximately 70 iterations.
The best array obtained (SLL = -20.52 dB) is given below as a status table ($on = 1$, $off = 0$) for half of the elements (as the array is symmetric):

1 1 1 1 1 1 1 1 1 1 1 1 1 1 1 1 1 1 1 1 1 1 1 1 1
1 0 1 1 1 1 0 0 1 0 1 0 0 1 1 1 1 1 0 0 1 0 0 1 1

3.2.2.2 Planar array

As a final example, we will now deal with the design of a thinned planar array. The SLL level will be checked in the two main planes of the array. To this aim, we have used the desirability function given below:

$$\eta_j = min(|SLL_{\phi=0}(dB)|, |SLL_{\phi=90}(dB)|) \tag{12}$$

Figure 11 shows the result obtained with 10 ants, 100 iterations and 20×10 elements. The food is considered to be -24 dB of SLL in each plane ($\phi = 0^\circ$ and $\phi = 90^\circ$). The algorithm has a fast convergence (in approximately 40 iterations).
The achieved solution is given below as a status table for one quadrant (x-positive in horizontal and y-positive in vertical) of the elements (the obtained SLLs are -25.76 dB and -25.67 dB for planes $\phi = 0^\circ$ and $\phi = 90^\circ$, respectively):

1 1 1 1 1 1 1 1 1 1
1 1 1 1 1 1 1 1 1 0
1 1 1 1 1 1 1 0 0 0
1 1 1 1 1 0 0 0 0 0
1 1 1 0 0 0 0 0 0 0

After all the presented examples we can stand that ACO has demonstrated to be an useful optimization tool for array design, but also, since it can provide a good solution with low number of iterations and a low population, it could be a good candidate for solving more complex electromagnetic problems where the evaluation of the fitness function has a high computational cost (since a full wave simulation is typically required) as it will be shown in the following Sections.

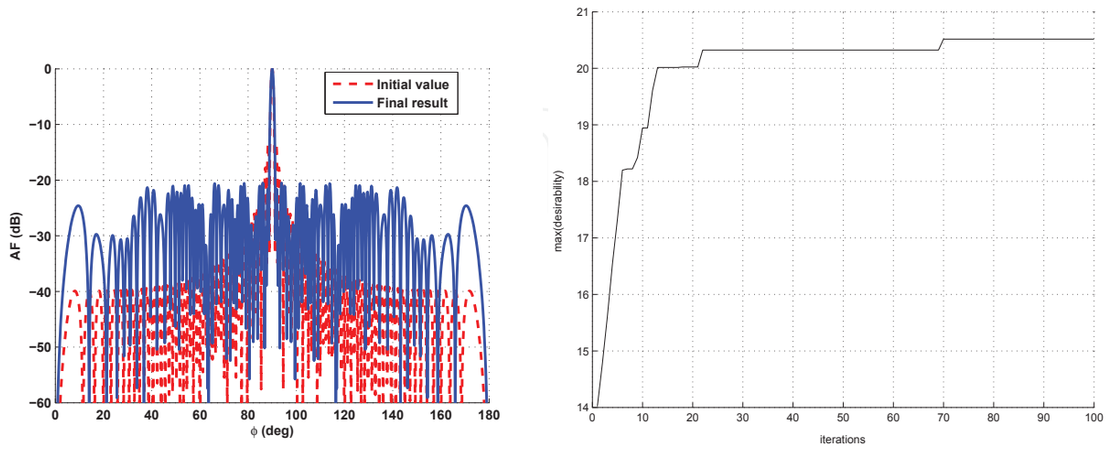

(a) Radiation pattern (b) Convergence

Fig. 9. Radiation pattern and convergence of a *100*-element array obtained by the ant algorithm (dashed line) compared to the initial value (solid line). ($SLL < -20\,\mathrm{dB}$)

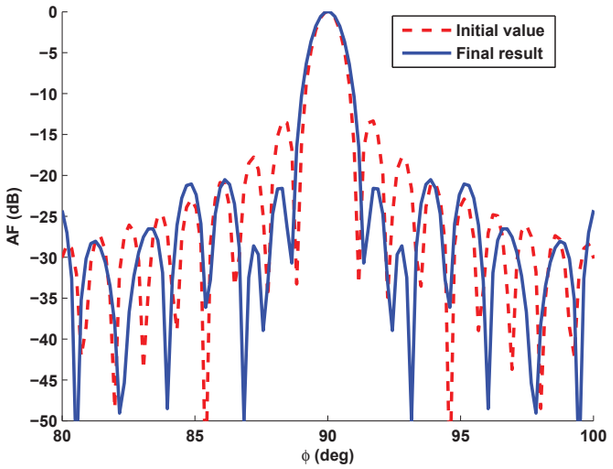

Fig. 10. Detail of the Array Factor (AF) shown in Figure 9.a.

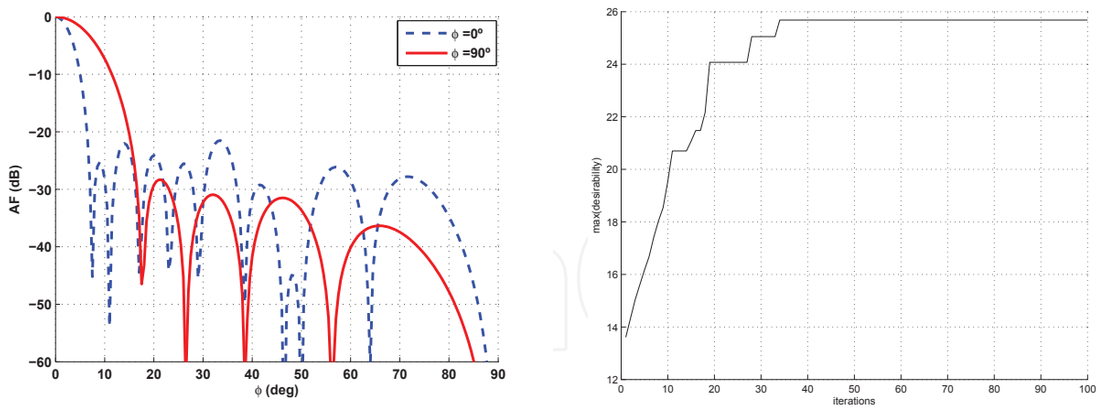

(a) Radiation pattern (b) Convergence

Fig. 11. Radiation pattern and convergence of 10×20-element planar array in the planes $\phi = 0^\circ$ and $\phi = 90^\circ$. ($SLL < -24$ dB in both planes)

3.3 Mutual coupling reduction in patch antenna arrays by using a planar EBG

The first problem in which we are going to use the ACO algorithm combined with a commercial full wave simulator is the reduction of mutual coupling between patch antennas by using a periodic structure (Electromagnetic Band Gap (EBG) type).

Mutual coupling reduction in arrays has deserved much attention from antenna designers. This coupling becomes especially critical in arrays of patch antennas where coupling comes from two sources (Pozar (1987), Bamford et al. (1997)). The first one is due to the free space radiation which is present in all types of array antennas. The second path arises from surface waves and it constitutes a very important factor in patch antennas (James & Hall (1997), Pozar & Schaubert (1995)). Moreover, the use of thick or high permittivity substrates increases the coupling.

Periodic structures such as EBGs have the ability of suppressing surface waves propagation in a frequency band. Consequently, their use in mutual coupling reduction for printed antennas can be of interest. For the particular case of patch antennas, the reduction of mutual coupling by using a periodic structure becomes particularly challenging when grating lobes must be avoided, since the distance between the edges of two neighboring patches is very small under this no grating lobes constraint.

For this reason, most of the proposals in the literature to reduce the coupling use a high permittivity dielectric and a modest number of periods of the structure in between the array elements. This means that this is a very challenging problem and the use of an optimization tool could be very helpful. In (Yang & Rahmat-Samii (2009)), the authors recognize this difficulty, and they made use of PSO to carry out the optimization of the periodic structure. In this section we will employ ACO for the same purpose.

Most of the previous works related to mutual coupling reduction for printed antennas are aimed at EBGs non completely planar, as it is the case of (Yang & Rahmat-Samii (2003), Yang et al. (2005), Fu & Yuan (2004), Zheng et al. (2008) and Caminita et al. (2009)). Besides, all of them use thin high permittivity substrates and both the periodic structure and the patch antenna are printed on the same layer. Our purpose is to provide another approach in the mutual coupling reduction for patch antennas by using completely planar EBGs.

One of the key aspects for this design is the use of a multilayer dielectric substrate (Chiau et al.

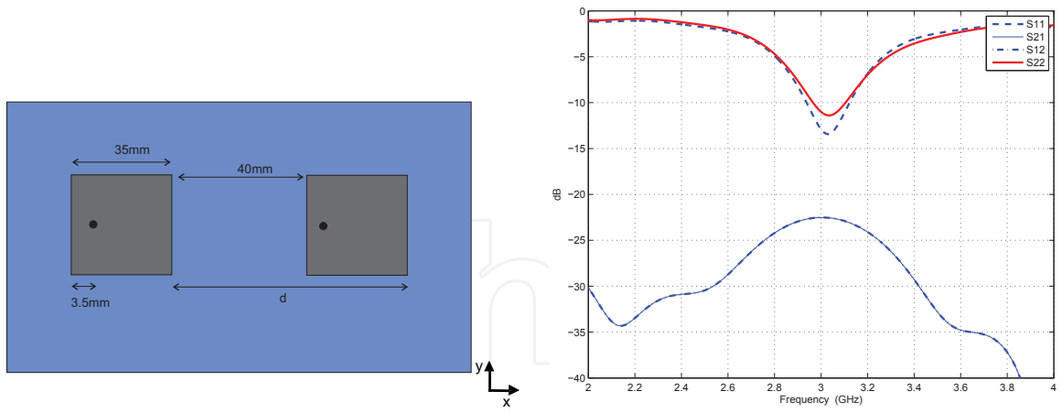

(a) Antenna top view (b) S parameters

Fig. 12. Simulated mutual coupling between antennas and input impedance of both antennas.

(2003), Inclán-Sánchez et al. (2005), Rajo-Iglesias et al. (2008)). With the combination of high permittivity and low permittivity dielectric layers, we can print the patch antenna and the EBG in different substrates (the EBG on the high permittivity material for the sake of compactness and the antenna on the low permittivity one for increasing the radiation efficiency). The advantages of this configuration will be further discussed.
A basic type of planar EBG, made of metallic patches printed on a grounded dielectric substrate, is the proposed periodic structure to be used for mutual coupling reduction (Yang et al. (2000), Goussetis et al. (2006)).

3.3.1 Initial design

In this section, we define a starting point for the subsequent optimization. The chosen EBG (Goussetis et al. (2006)) is not so compact and consequently most of the authors employ a high permittivity substrate. Here, we will use a material with $\epsilon_r \simeq 10$ and a 2.54 mm thickness.
Unfortunately, this substrate will produce an antenna with a low bandwidth as well as a moderate directivity (James & Hall (1997)). Consequently, we propose a multilayer dielectric structure. The EBG will be placed above the high permittivity lower layer, obtaining a structure with a reduced size. Over the latter, the second layer with a low permittivity and thick thickness will be located for achieving an equivalent low permittivity to the patches, which will be placed above this upper substrate. This multilayer configuration is inspired in the work presented in (Inclán-Sánchez et al. (2005)). The chosen upper layer will have an $\epsilon_r \simeq 1$ and 6 mm thickness.
To study the mutual coupling between array elements, we will employ a basic configuration with two patch antennas. The antennas will be designed to work at 3 GHz. The dimensions of the patches and the distances between them are illustrated in Figure 12.a. For this structure, the simulated mutual coupling (S_{12}) is represented in the same Figure, with the input impedance as a reference for the operating frequency. Both antennas are well matched (with a S_{11} and S_{22} smaller than -10 dB), and the maximum mutual coupling is approximately -23 dB.
The EBG unit cell is illustrated in Figure 13.a. The initial chosen dimensions for the EBG following (Goussetis et al. (2006)) are $d_x = d_y = 15$ mm and $p_x = p_y = 25$ mm. Considering this structure infinite we can obtain its associated dispersion diagram represented in Figure 13.b. The two blue lines correspond to the two first modes propagating in the structure, and

the dashed red line represents the light line. We can conclude that there is a band around 3 GHz where the propagation in x direction is not allowed.
This is however a theoretical study, assuming infinite number of cells in the EBG. For the proposed application it is necessary to truncate the EBG and only two lines of elements will fit between the patches in the E-plane, whilst in the H-plane, in principle, there is no constraint. This fact limits the characteristics of our filtering structure.
After these previous considerations, we are able to define the complete antenna with the EBG for the mutual coupling reduction. The scheme of this design is shown in Figure 14.a with the side and top views of an array of two elements. We have initially considered four elements in the H-plane for the compactness of the design. Figure 14.b shows the S parameters for the complete structure. A considerable reduction of the mutual coupling has been achieved, with a maximum of -29 dB, that is 6 dB less than in the previous case without the EBG (Figure 12.b). Moreover, the antennas are even better matched than in the case without EBG, having a higher total antenna efficiency.

3.3.2 Definition of the ant colony algorithm parameters

Although we have obtained a considerable reduction of the mutual coupling (approximately 6 dB), an optimization with an ACO algorithm is now carried out to further improve these results. As previously mentioned, this algorithm fits properly with this problem where a good initial solution has already been obtained. The parameters to be optimized are the dimensions of the cells and the distance between them: d_x, d_y, p_x and p_y. These parameters have as constraint the space between the patches, not being allowed to overlap the volume defined by the patches. The goal for the optimization will be the maximum reduction of the mutual coupling.
The chosen parameters for this optimization problem, have been the following: $\gamma = 20$, $\rho = 1$, $\alpha = 30$, $\beta = 2$. These parameters have been selected heuristically. The chosen desirability was the module of S_{21} at the operation frequency of patches (at the lowest value of S_{11}).
The algorithm was developed in *MATLAB*© and employed *CST*© commercial software as analysis tool (in transient solver) to calculate the mutual coupling between the patches. Each ant must calculate the desirability of all the neighboring nodes (defined by increasing and decreasing one step each of the 4 parameters to optimize). With this value of desirability as

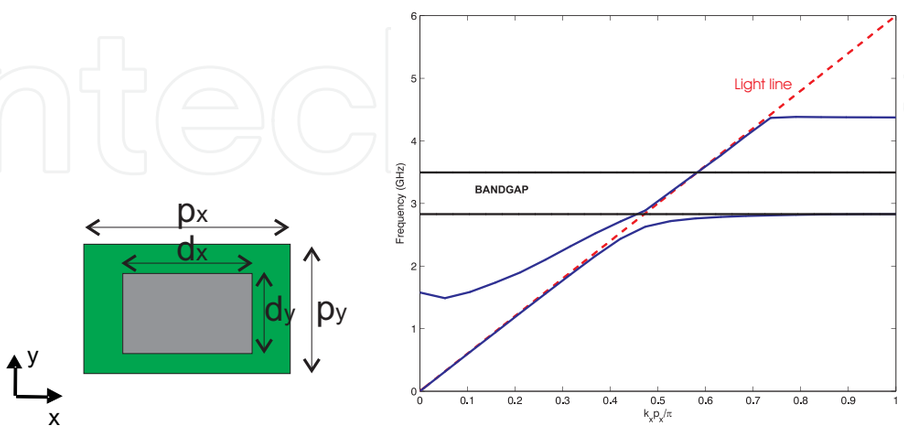

(a) EBG unit cell (b) Dispersion diagram

Fig. 13. Dispersion diagram of the EBG (represented in E-plane direction).

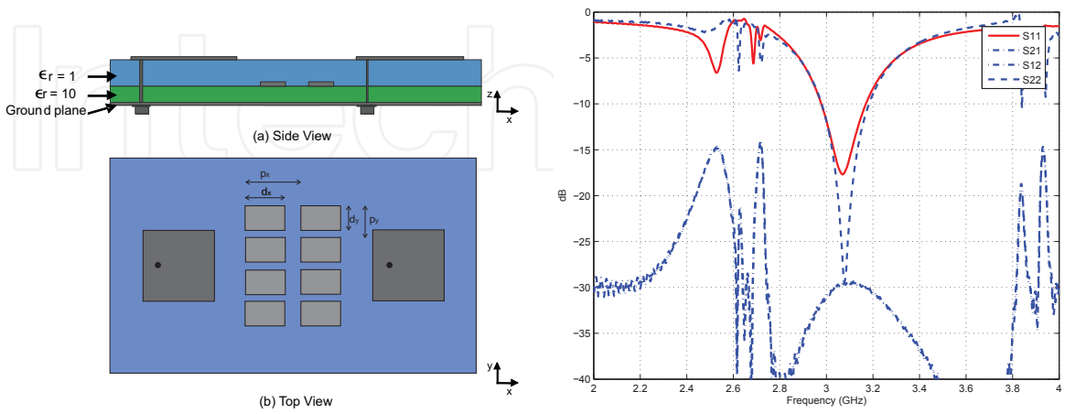

(a) Description of the geometry (b) S parameters

Fig. 14. Simulated mutual coupling and matching for the array with EBG.

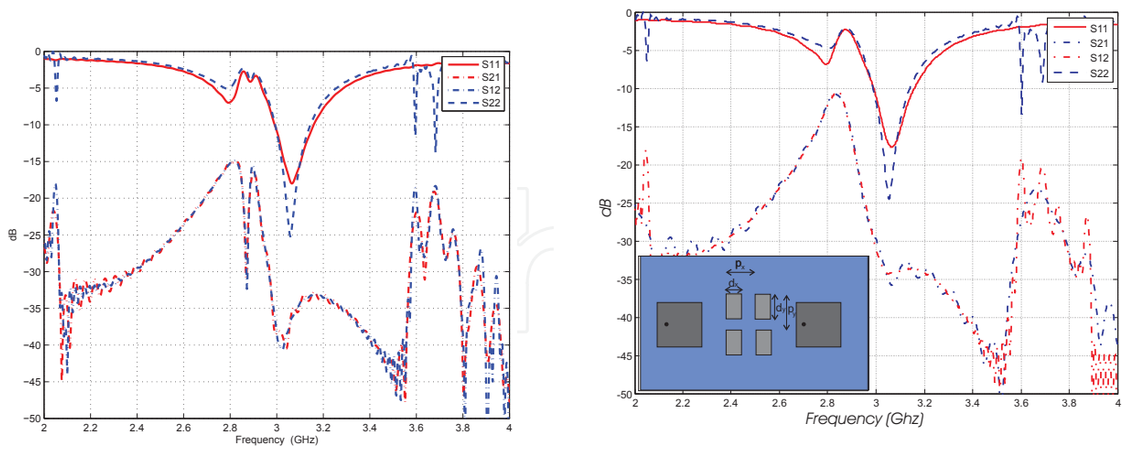

(a) 8 element EBG. (b) 4 element EBG.

Fig. 15. Simulated mutual coupling for the array with optimized EBG.

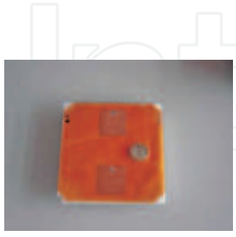

(a) Manufactured *two*-element multilayer array

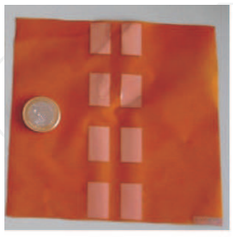

(b) Planar periodic 8-element EBG

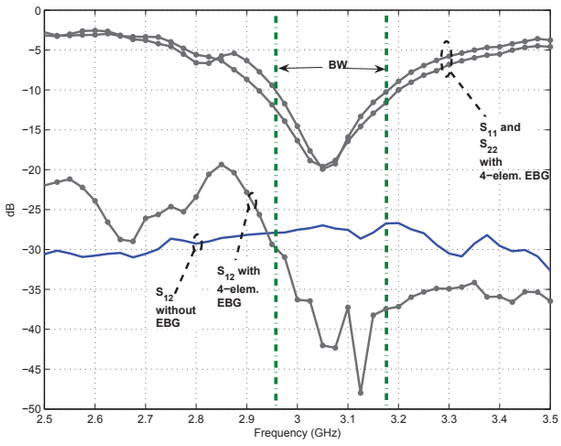

(c) Measured S parameters: with and without EBG

Fig. 16. Experimental mutual coupling for the array with optimized EBG.

well as with the pheromone concentration, each ant makes the decision of moving to a new position with the probability expression defined in Equation 1.

3.3.3 Optimized results

After several iterations, the obtained dimensions were $d_x = 13\,\text{mm}$, $d_y = 22\,\text{mm}$, $p_x = 20\,\text{mm}$ and $p_y = 35\,\text{mm}$. Figure 15(a) shows the simulated result obtained for these dimensions. The mutual coupling is below -35 dB. This means that the mutual coupling reduction is approximately 6 dB if we compare with the case before optimization, and 12 dB with the structure without EBG. Looking for the most compact design in H-plane, in Figure 15(b), we illustrate the simulated results for a structure with only 4 elements as the inset of this Figure shows.

3.3.4 Experimental results

In order to validate the results obtained by the previous simulations, some prototypes were manufactured. In Figure 16, we show a photograph of the structure with the patches including a multilayer substrate and the EBG, as well as the picture of the layer with the eight printed metallic elements.

In Figure 16.c, the measured parameter S_{12} is illustrated for the case of 4-elements with the band within which S_{11} is below -10 dB defined by the two vertical dashed lines. In most parts of the band, a reduction of the mutual coupling by more than 10 dB is achieved and the EBG does not affect the matching of the antennas.

3.4 Split ring resonators loaded on the sidewalls of rectangular waveguides

The next example will deal with how to operate ordinary waveguides below its cutoff frequency to get miniaturized structures (Hrabar et al. (2005), Kehn et al. (2006)). We show now a possible solution based on Split Ring Resonators (SRR) (Quevedo-Teruel et al. (2009)) that has been designed by using an ACO algorithm. This is a problem where the proposed ACO algorithm is especially convenient as the computational cost of the evaluation of each solution is very high.

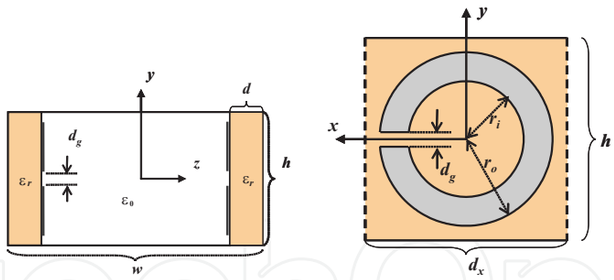

(a) Waveguide cross section (b) SRR dimensions

Fig. 17. Geometry of the analyzed waveguide.

The possibility of operating the waveguide below its usual fundamental modal cutoff frequency provides miniaturization of the structure (Falcone et al. (2004), Marqués et al. (2002), Burokur et al. (2007), Esteban et al. (2005), Quevedo-Teruel et al. (2009)). To this aim, in the work of (Hrabar et al. (2005)), the waveguide was loaded with arrays of SRR printed on both sides of a centrally located dielectric slab. Instead, in this work we propose to place these SRRs on the lateral sidewalls as Figure 17 shows. This structure is inspired in the one investigated in (Kehn et al. (2006)), in which an array of rectangular patches is printed on the surface of each sidewall dielectric of a rectangular waveguide for obtaining a TEM behavior. This unusual effect of propagation below cutoff will be only produced in a narrow band where the SRRs resonate, being possible to tune that resonant frequency below or above the cutoff frequency of the dominant ordinary waveguide mode of the structure. Below, backward passband will be achieved, whereas above the cutoff frequency, these waveguides will exhibit stopbands (Shelkovnikov & Budimir (2006), Jitha et al. (2006), Rajo-Iglesias et al. (2009), Kehn et al. (2008)).

In this section we study the case of SRR loadings in the waveguide sidewalls using again an Ant Colony Optimization algorithm to optimize the SRR parameters for achieving the lowest operation frequency of the backward travelling modal passband that is significantly below the cutoff frequency of the dominant mode. The schematic of this SRR-loaded rectangular waveguide is shown in Figure 17.

3.4.1 Dispersion diagrams

Before the optimization, numerical studies of the proposed waveguide were developed in (Quevedo-Teruel et al. (2009)). To this aim, different values of the main parameters of the structure shown in Figure 17 were analyzed by making use of dispersion diagrams obtained with the eigenvalue analyzer of *CST Microwave Studio*© which requires a high computational cost.

An example of the dispersion curves obtained from simulations is shown in Figure 18. With reference to Figure 17, the example is for a configuration with a waveguide width w of 20 mm, height h of 10 mm and a period d_x of 10 mm along $\hat{x}$. The thickness d of the dielectric slab is 2 mm, and its relative permittivity $\epsilon_r = 3.2$. For the SRR, which is geometrically centered within the unit cell, its outer radius r_o is 4 mm, inner radius r_i is 3.2 mm, and the gap distance d_g is 1 mm.

Two narrow backward-modal passbands appear around 4.2 GHz as Figure 18 shows. This is then followed by a stopband from around 4.5 GHz to 7.5 GHz, beyond which the dominant mode appears. The second mode also re-emerges at a higher frequency. Hence, each of the

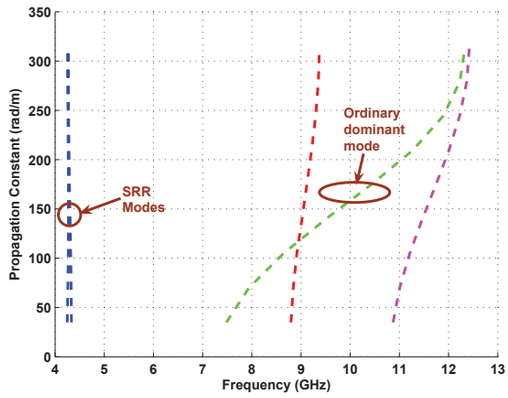

Fig. 18. Dispersion diagram of SRR-waveguide, loaded with a dielectric material of $\epsilon_r = 3.2$, with dimensions: $w = 20\,\text{mm}$, $h = 10\,\text{mm}$, $d_x = 10\,\text{mm}$, $d = 2\,\text{mm}$, $r_o = 4\,\text{mm}$, $r_i = 3.2\,\text{mm}$, and $d_g = 1\,\text{mm}$.

two dominant modes first appears as a backward travelling mode within a low and narrow passband, goes to cutoff, and then reappears as ordinary modes in the higher band.

3.4.2 Optimized design

After this previous example, we now deal with a real design where the dimensions of the supporting waveguide are established to be the standard *C*-band type whose cross-sectional dimensions are $3.5\,\text{cm} \times 1.6\,\text{cm}$. The material on which the SRR array is printed has been selected to be conventional fiber glass with $\epsilon_r = 4.5$, loss tangent 0.012 and with 1.55 mm thickness.

The proposed optimization goal is to achieve the new passband below ordinary waveguide cutoff at the lowest possible frequency. This is intended for possible miniaturization purposes. Therefore, we employed an ACO algorithm, making use of the following parameters for the optimization: the SRR dimensions, i.e. inner and outer radii, gap of the SRR and period of the unit cell. The desirability function employed for this optimization was the following:

$$\eta_j = (10 - median(\{f_i\}/10^9)) \tag{13}$$

in which $\{f_i\}$ represents the set of frequencies that allows the propagation of the mode that is being targeted for minimization of its passband frequency. For each frequency in this set, there is an associated propagation constant of that considered mode. The aim of the algorithm is to maximize this function, and hence, to minimize the frequency of the backward mode. The index j of η denotes the case index, where each case pertains to a certain set of optimization parameters.

In this case, the eigenmode solver of *CST*© is used as the analysis tool to compute the dispersion diagrams for solution evaluation; and as previously, ACO was implemented in *MATLAB*© which uses *CST*© to evaluate the goodness of the solutions. As a consequence, this process will be computationally heavy. Therefore, both a moderate number of ants and iterations have been used. As mentioned before, this fact provides a lower computational time than other global search algorithms (for example genetics) where the number of individuals must be much higher to achieve good results. In order to decide the movement of each ant, the algorithm has to compute the dispersion diagrams of all the neighboring nodes. As 4

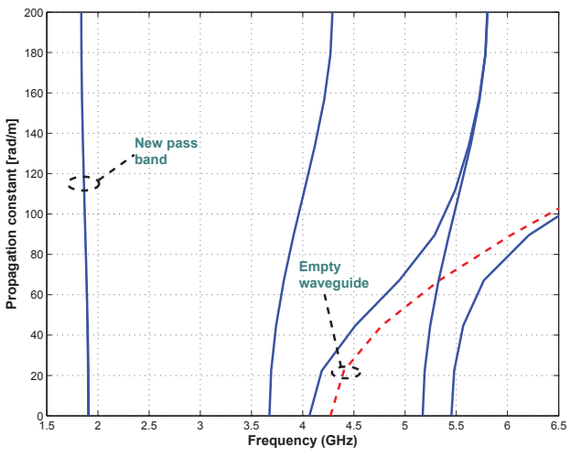

Fig. 19. Dispersion diagram of the optimized waveguide and comparison with the waveguide without SRR (red dashed line).

parameters are used for optimization, each ant movement requires the evaluation of 8 possible solutions.

After several iterations of the optimization algorithm, the final optimized SRR dimensions are r_i: 6.4mm, r_o: 7.6mm, d_g: 1.4mm and unit cell period: 15.6mm. With these dimensions the dispersion diagram is the one shown in Figure 19. There is a backward mode at a low frequency of approximately 1.8GHz. For the sake of comparison, the dispersion diagram of the same waveguide with the dielectric loaded walls but without the SRR loading is shown in the same Figure 19, in which a total absence of propagating modal passbands below the waveguide cutoff is clear. In the presented frequency range, three additional modes appear as a consequence of the SRR loading.

The dispersion diagram for the SRR loaded waveguide with the optimized SRR dimensions shows a narrow passband near 2GHz, whilst the original waveguide cutoff is slightly over 4GHz. Thus a significant degree of miniaturization has been achieved.

3.4.3 Experimental results

A demonstrator has been manufactured whose dimensions correspond to the ones described in the previous section for the optimized case. Figure 20.a shows a picture of the manufactured waveguide with the top wall open in order to show the SRR array of 12 elements which is placed on each wall. As the field of the SRR-attributed modes is weak in the center of the waveguide, the feeding system consists of two vertical probes allocated close to the lateral walls, i.e., close to the SRR. These two probes for each port, were excited with a rat-race that was designed at the operation frequency (Quevedo-Teruel et al. (2009)).

At the operation frequency, both even and odd modes are, in principle, possible. The rat-race is used to divide the signal in two ports with the same phase or a 180° difference, obtaining an even or odd mode, respectively. The two rat-races were placed at each end of the waveguide and the transmission coefficient between them (S_{12}) was measured. The measurement results are presented in Figure 20.b for the frequency range in which the new passband is created. The odd mode presents a higher level of transmission when compared to the even one. In the figure, the results for the same waveguide but without the SRR loadings are included for comparison purposes. Although the transmission is low, it is still 30dB higher than the levels outside the new SRR-attributed passband. Hence, this new transmission band which would

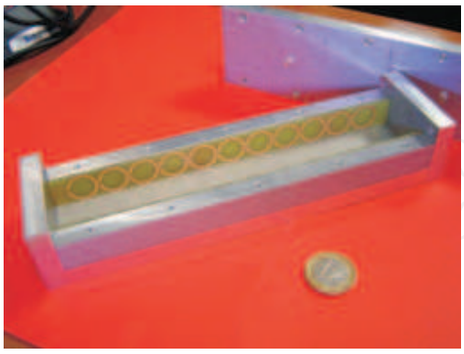

(a) Manufactured waveguide

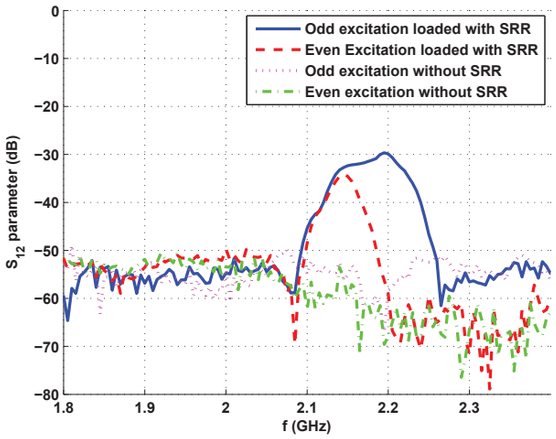

(b) S_{21}

Fig. 20. Measured transmission coefficient with and without SRR loading.

otherwise be absent in the empty waveguide, is clearly verified in these experimental results. The main reason for the low transmission is the mismatch due to the difference between the impedance of the experimental waveguide and the port impedance of the employed feeding probe.

3.5 Monopolar ultra wide band (UWB) microstrip antenna

As a last example of application of the ACO algorithm, an optimization of a monopolar UWB microstrip antenna is presented. Printed monopolar-type UWB antennas are becoming more and more popular. They can have many different shapes, as for instance the PICA (Planar Inverted Cone Antenna, Suh et al. (2004)), rectangular (Choi et al. (2004)), or circular disc. This type of antennas (in its both feeding versions: microstrip and co-planar) have been extensively studied (Liang et al. (2004), Lin & Huang (2005), Ren & Chang (2006), Suh et al. (2005)), due to their broadband and planar nature and hence, a low cost of manufacturing and low weight. However, the design of these antennas is not trivial, and a parametric study is not always enough since their parameters do not scale linearly in different frequency bands. Consequently, an optimization process is often convenient to obtain a design that fulfills given requirements.

As an example, a particular microstrip monopolar antenna has been optimized. The antenna is represented in Figure 21.a. The optimization goal is to get S_{11} below -10 dB in the largest possible band. To achieve this aim an ACO algorithm is employed together with the transient solver of $CST^{©}$ for obtaining the S_{11} of the antenna. A possible desirability function, for the design of such an antenna in a certain band is the one shown in Equation 14 where N represents the number of frequency points obtained by the simulation tool whose S_{11} values are above -10 dB in the band under study.

$$\eta_j = \frac{1}{N} \cdot \sum_{n=1}^{N} (10 - |S_{11}(f_n)|) \tag{14}$$

In this case, the following variables are chosen for optimization: the radii (r and R), the length of the ground plane (L), the width of the feeding line (W) and the distance between the circle

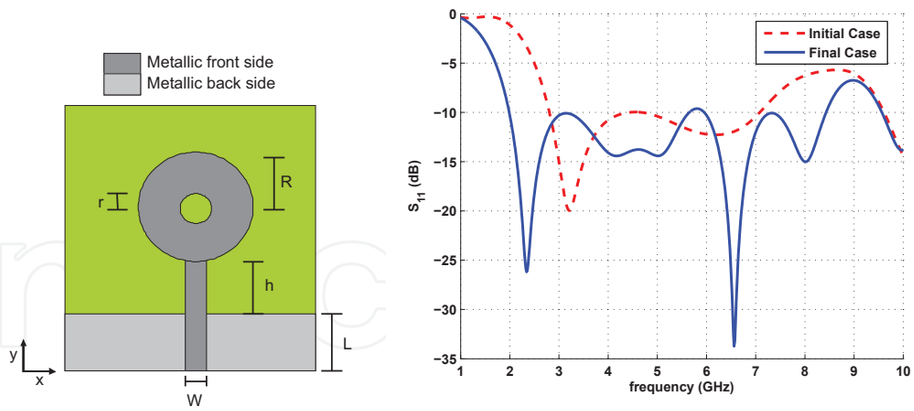

(a) Antenna geometry (b) S_{11}

Fig. 21. Monopolar UWB microstrip antenna and simulated return losses before and after optimization.

and the ground plane (h). The food has been established to be 11, in order to be all the time in the *forward way* of the ACO algorithm. The number of ants was 10 and the optimization parameters were: $\alpha = 1$ and $\beta = 30$. The discrete step of variation was 0.5mm. Figure 21.b shows the initial and optimized S_{11} for the studied antenna for a band between 2 and 8GHz with fiber glass as dielectric ($\epsilon_r = 4.5$ with 1.55mm thickness).
The best obtained result has the following parameters: $R = 14.5$mm, $r = 2.5$mm, $h = 0.5$mm, $L = 20$mm and $W = 2.6$mm. Figure 22 shows a photograph of the manufactured prototype and a comparison between simulations and measurements associated to this prototype. This antenna fulfills the S_{11} requirements in the frequency band between 2 and 8GHz. The simulated radiation patterns for this antenna at different frequencies are plotted in Figure 23. The radiation patterns have some variations when the frequency increases, since the optimization was developed only in terms of return losses.

4. Conclusion

In this chapter we have shown the possibilities of ACO algorithm for solving electromagnetic problems. Several examples illustrate the advantages of using this algorithm. Initially we have explored the possibilities of the algorithm for a classical optimization problem in electromagnetism: the array synthesis. We have shown through different examples how the ACO algorithm is as useful as other types of algorithms such as Genetics or Particle Swarm to be applied in this type of problems.
However the interesting performance of this algorithm for electromagnetic designs is shown with examples where the evaluation of the goodness of a potential solution is computationally very costly. Three examples of such type of problems have been as well studied along this chapter. In all of them the implemented algorithm was able of outperform an initial good solution obtained after parametric studies. This demonstrates the enormous potential of the algorithm in this field of application.

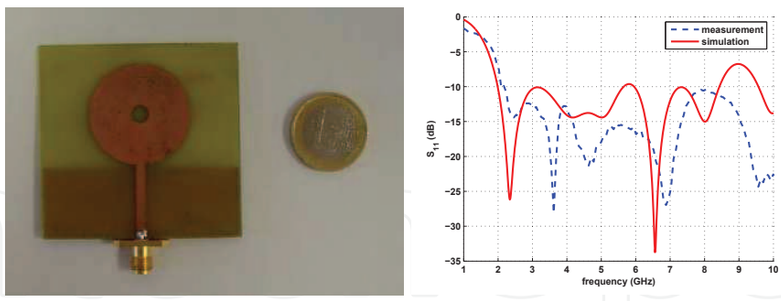

(a) Manufactured prototype (b) S_{11}

Fig. 22. Measured S_{11} parameter after optimization for the monopolar UWB microstrip antenna

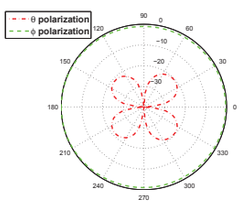

(a) $\phi = 0°$ (2GHz)

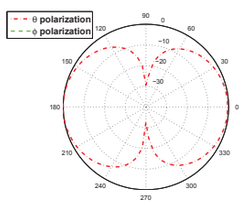

(b) $\phi = 90°$ (2GHz)

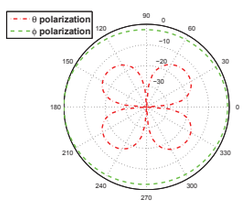

(c) $\phi = 0°$ (3GHz)

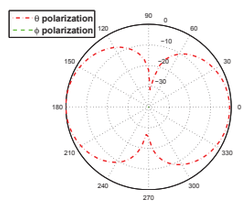

(d) $\phi = 90°$ (3GHz)

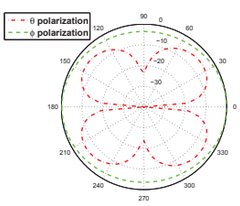

(e) $\phi = 0°$ (4GHz)

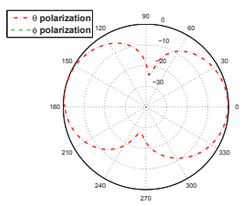

(f) $\phi = 90°$ (4GHz)

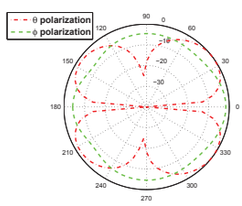

(g) $\phi = 0°$ (5GHz)

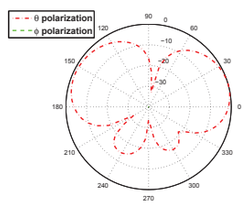

(h) $\phi = 90°$ (5GHz)

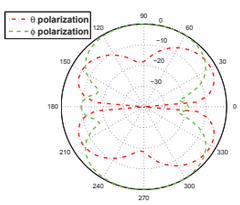

(i) $\phi = 0°$ (6GHz)

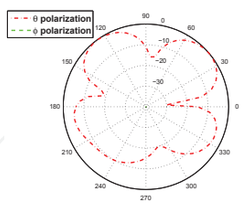

(j) $\phi = 90°$ (6GHz)

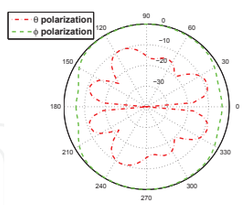

(k) $\phi = 0°$ (7GHz)

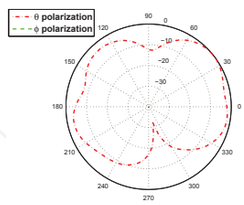

(l) $\phi = 90°$ (7GHz)

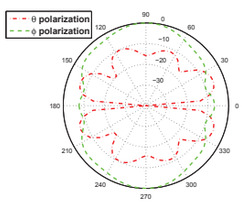

(m) $\phi = 0°$ (8GHz)

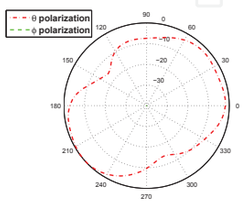

(n) $\phi = 90°$ (8GHz)

Fig. 23. Simulated radiation patterns of the optimized monopolar UWB Microstrip Antenna.

5. References

Ahuja, A. & Pahwa, A. (2005). Using ant colony optimization for loss minimization in distribution networks, *Proceedings of the 37th Annual North American Power Symposium*, pp. 470–474.

Ares-Pena, F. J., Rodriguez-Gonzalez, J. A., Villanueva-Lopez, E. & Rengarajan, S. R. (1999). Genetic algorithms in the design and optimization of antenna array patterns, *IEEE Transactions on Antennas and Propagation* 47(3): 506–510.

Bamford, L. D., James, J. R. & Fray, A. F. (1997). Minimising mutual coupling in thick substrate microstrip antenna arrays, *Electronics Letter* 33(8): 648–650.

Bullnheimer, B., Hartl, R. & Strauss, C. (1999). A new rank based version of the ant system - a computational study, *Central Eur. J. Oper. Res. Econ.* 7(1).

Burokur, S. N., Latrach, M. & Toutain, S. (2007). Influence of split ring resonators on the properties of propagating structures, *IET Microwaves, Antennas and Propagation* 1(1): 94–99.

Caminita, F., Costanzo, S., Di Massa, G., Guarnieri, G., Maci, S., Mauriello, G. & Venneri, I. (2009). Reduction of patch antenna coupling by using a compact EBG formed by shorted strips with interlocked branch-stubs, *IEEE Antennas and Wireless Propagation Letters* 8: 811–814.

Chiau, C., Chen, X. & Parini, C. (2003). A microstrip patch antenna on the embedded multi-period EBG structure, *Proceedings of 6th International Symposium on Antennas, Propagation and EM Theory, 2003.*, pp. 96–99.

Choi, S. H., Park, J. K., Kim, S. K. & Park, J. Y. (2004). A new ultra-wideband antenna for UWB applications, *Microwave and Optical Technology Letters* 40: 339–401.

Coleman, C. M., Rothwell, E. J. & Ross, J. E. (2004). Investigation of simulated annealing, ant-colony optimization, and genetic algorithms for self-structuring antennas, *IEEE Transactions on Antennas and Propagation* 52(4): 1007–1014.

Dorigo, M., Birattari, M., Blum, C., Gambardella, L. M., Mondada, F. & Sttzle, T. (2004). *Ant Colony Optimization and Swarm Intelligence*, Springer.

Dorigo, M., Caro, G. D. & Gambardella, L. M. (1999). Ant algorithms for discrete optimization, *Artificial Life* 5(2): 137–172.

Dorigo, M., Maniezzo, V. & Colorni, A. (1996). Ant system: Optimization by a colony of cooperating agents, *IEEE Transactions on Systems, MAN, and Cybernetics-Part B* 26(1): 29–41.

Dorigo, M. & Stutzle, T. (2004). *Ant Colony Optimization*, The MIT Press.

Esteban, J., Camacho-Penalosa, C., Page, J., Martin-Guerrero, T. & Marquez-Segura, E. (2005). Simulation of negative permittivity and negative permeability by means of evanescent waveguide modes-theory and experiment, *IEEE Transactions on Microwave Theory and Techniques* 53(4): 1506–1514.

Falcone, F., Martin, F., Bonache, J., Marqués, R., Lopetegi, T. & Sorolla, M. (2004). Left handed coplanar waveguide band pass filters based on bi-layer split ring resonators, *IEEE Microwave and Wireless Component Letters* 14(1): 10–12.

Fu, Y. & Yuan, N. (2004). Elimination of scan blindness in phased array of microstrip patches using electromagnetic bandgap materials, *IEEE Antennas and Wireless Propagation Letters* 3: 64–65.

Goussetis, G., Feresidis, A. & Vardaxoglou, J. (2006). Tailoring the AMC and EBG characteristics of periodic metallic arrays printed on grounded dielectric substrate, *IEEE Transactions on Antennas and Propagation* 54(1): 82–89.

Haupt, R. L. (1994). Thinned arrays using genetic algorithms, *IEEE Transactions on Antennas and Propagation* 42(7): 993–999.

Haupt, R. L. (2005). Interleaved thinned linear arrays, *IEEE Transactions on Antennas and Propagation* 53(9): 2858–2864.

Haupt, R. L. & Werner, D. H. (2007). *Genetic Algorithms in Electromagnetics*, Wiley.

Hoshyar, R., Jamali, S. H. & Locus, C. (2000). Ant colony algorithm for finding good interleaving pattern in turbo codes, *IEE Proceedings on Communications* 147(5): 257–262.

Hrabar, S., Bartolic, J. & Sipus, Z. (2005). Waveguide miniaturization using uniaxial negative permeability metamaterial, *IEEE Transactions on Antennas and Propagation* 53(1): 110–119.

Inclán-Sánchez, L., Rajo-Iglesias, E., González-Posadas, V. & Vázquez-Roy, J. (2005). Design of periodic metallo-dielectric structure for broadband multilayer patch antenna, *Microwave and Optical Technology Letters* 44(5): 418–421.

James, J. R. & Hall, P. S. (1997). *Handbook of Microstrip and Printed Antennas*, New York: Wiley.

Jin, N. & Rahmat-Samii, Y. (2007). Advances in particle swarm optimization for antenna designs: Real-number, binary, single-objective and multiobjective implementations, *IEEE Transactions on Antennas and Propagation* 55(3): 556–567.

Jitha, B., Nimisha, C. S., Aanandan, C. K., Mohanan, P. & Vasudevan, K. (2006). SRR loaded waveguide band rejection filter with adjustable bandwidth, *Microwave and Optical Technology Letters* 48(7): 1427–1429.

Kehn, M. N. M., Nannetti, M., Cucini, A., Maci, S. & Kildal, P.-S. (2006). Analysis of dispersion in dipole-FSS loaded hard rectangular waveguide, *IEEE Transactions on Antennas and Propagation* 54(8): 2275–2282.

Kehn, M., Quevedo-Teruel, O. & Rajo-Iglesias, E. (2008). Split-ring resonator loaded waveguides with multiple stopbands, *Electronics Letters* 44(12): 714–716.

Khodier, M. M. & Christodoulou, C. G. (2005). Linear array geometry synthesis with minimun sidelobe level and null control using particle swarm optimization, *IEEE Transactions on Antennas and Propagation* 53(8): 2674–2679.

Liang, J., Chiau, C. C., Chen, X. & Parini, C. G. (2004). Printed circular disc monopole antenna for ultra-wideband applications, *Electronic Letters* 40(20): 1246–1247.

Liang, Y.-C. & Smith, A. E. (2004). An ant colony optimization algorithm for the redundancy allocation problem (RAP), *IEEE Transactions on Reliability* 53(3): 417–423.

Lin, S.-Y. & Huang, K.-C. (2005). A compact microstrip antenna for GPS and DCS application, *IEEE Transactions on Antennas and Propagation* 53(3): 1227–1229.

Marqués, R., Martel, J., Mesa, F. & Medina, F. (2002). Left-handed media simulation and transmission of EM waves in sub-wavelength SRR-loaded metallic waveguides, *Physical Review Letters* 89(18): 183901/1–4.

Pozar, D. M. (1987). Radiation and scattering from a microstrip patch on a uniaxial substrate, *IEEE Transactions on Antennas and Propagation* 35(6): 613–621.

Pozar, D. M. & Schaubert, D. H. (1995). *Microstrip Antennas: The Analysis and Design of Microstrip Antennas and Arrays*, Wiley-IEEE Press.

Premprayoon, P. & Wardkein, P. (2005). Topological communication network design using ant colony optimization, *The 7th International Conference on Advanced Communication Technology*, Vol. 2, pp. 1147–1151.

Quevedo-Teruel, O. & Rajo-Iglesias, E. (2006). Ant colony optimization in thinned array synthesis with minimum sidelobe level, *IEEE Antennas and Wireless Propagation*

Letters 5: 349–352.
Quevedo-Teruel, O., Rajo-Iglesias, E. & Kehn, M. N. M. (2009). Numerical and experimental studies of split ring resonators loaded on the sidewalls of rectangular waveguides, *IET Microwaves, Antennas and Propagation* 3(8): 1262–1270.
Quevedo-Teruel, O., Rajo-Iglesias, E. & Oropesa-Garcia, A. (2007). Hybrid algorithms for electromagnetic problems and the no-free-lunch framework, *IEEE Transactions on Antennas and Propagation* 55(3): 742–749.
Rajo-Iglesias, E. & Quevedo-Teruel, O. (2007). Linear array synthesis using an ant colony optimization based algorithm, *IEEE Antennas and Propagation Magazine* 49(2): 70–79.
Rajo-Iglesias, E., Quevedo-Teruel, O. & Inclán-Sánchez, L. (2008). Mutual coupling reduction in patch antenna arrays by using a planar EBG structure and a multilayer dielectric substrate, *IEEE Transactions on Antennas and Propagation* 56(6): 1648–1655.
Rajo-Iglesias, E., Quevedo-Teruel, O. & Kehn, M. (2009). Multiband SRR loaded rectangular waveguide, *IEEE Transactions on Antennas and Propagation* 57(5): 1571–1575.
Ren, Y.-J. & Chang, K. (2006). An annular ring antenna for UWB communications, *IEEE Antennas and Wireless Propagation Letters* 5: 274–276.
Robinson, J. & Rahmat-Samii, Y. (2004). Particle swarm optimization in electromagnetics, *IEEE Transactions on Antennas and Propagation* 52(2): 397–407.
Schwartzman, L. (1967). Element behavior in a thinned array, *IEEE Transaction on Antennas and Propagation* 15(4): 571–572.
Shelkovnikov, A. & Budimir, D. (2006). Left-handed rectangular waveguide bandstop filters, *Microwave and Optical Technology Letters* 48(5): 846–848.
Sim, K. M. & Sun, W. H. (2003). Ant colony optimization for routing and load-balancing: Survey and new directions, *IEEE Transactions on Systems, Man and Cybernetics, Part A* 33(5): 560–572.
Suh, S.-Y., Stutzman, W. & Davis, W. (2004). A new ultrawideband printed monopole antenna: The planar inverted cone antenna (PICA), *IEEE Transactions on Antennas and Propagation* 52(5): 1361–1364.
Suh, S.-Y., Stutzman, W. L., Davis, W. A., Waltho, A. E., Skeba, K. W. & Schiffer, J. L. (2005). A UWB antenna with a stop-band notch in the 5-ghz WLAN band, *IEEE/ACES International Conference on Wireless Communications and Applied Computational Electromagnetics*, pp. 203–207.
Tennant, A., Dawoud, M. & Anderson, A. (1994). Array pattern nulling by element position perturbations using a genetic algorithm, *Electronic Letters* 30(3): 174–176.
Wang, X.-N., Feng, Y.-J. & Feng, Z.-R. (2005). Ant colony optimization for image segmentation, *Proceedings of 2005 International Conference on Machine Learning and Cybernetics*, Vol. 9, pp. 5355–5360.
Yan, K. & Lu, Y. (1997). Sidelobe reduction in array-pattern synthesis using genetic algorithm, *IEEE Transactions on Antennas and Propagation* 45(7): 1117–1122.
Yang, F. & Rahmat-Samii, Y. (2003). Microstrip antennas integrated with electromagnetic band-gap (EBG) structures: A low mutual coupling design for array applications, *IEEE Transaction on Antennas and Propagation* 51(10): 2936 – 2946.
Yang, F. & Rahmat-Samii, Y. (2009). *Electromagnetic Band Gap Structures in Antenna Engineering*, Cambridge University Press.
Yang, H.-Y. D., Kim, R. & Jackson, D. R. (2000). Design consideration for modeless integrated circuit substrates using planar periodic patches, *IEEE Transactions on Microwave Theory and Techniques* 48(12): 2233–2239.

Yang, L., Fan, M., Chen, F., She, J. & Feng;, Z. (2005). A novel compact electromagnetic-bandgap EBG structure and its applications for microwave circuits, *IEEE Transactions on Microwave Theory and Techniques* 53(1): 183–190.

Zheng, Q.-R., Fu, Y.-Q. & Yuan, N.-C. (2008). A novel compact spiral electromagnetic band-gap (EBG) structure, *IEEE Transactions on Antennas and Propagation* 56(6): 1656–1660.

IntechOpen

IntechOpen

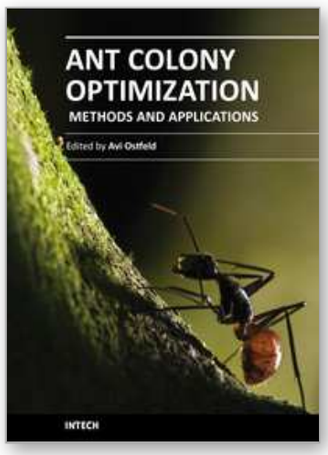

Ant Colony Optimization - Methods and Applications

Edited by Avi Ostfeld

ISBN 978-953-307-157-2
Hard cover, 342 pages
Publisher InTech
Published online 04, February, 2011
Published in print edition February, 2011

Ants communicate information by leaving pheromone tracks. A moving ant leaves, in varying quantities, some pheromone on the ground to mark its way. While an isolated ant moves essentially at random, an ant encountering a previously laid trail is able to detect it and decide with high probability to follow it, thus reinforcing the track with its own pheromone. The collective behavior that emerges is thus a positive feedback: where the more the ants following a track, the more attractive that track becomes for being followed; thus the probability with which an ant chooses a path increases with the number of ants that previously chose the same path. This elementary ant's behavior inspired the development of ant colony optimization by Marco Dorigo in 1992, constructing a meta-heuristic stochastic combinatorial computational methodology belonging to a family of related meta-heuristic methods such as simulated annealing, Tabu search and genetic algorithms. This book covers in twenty chapters state of the art methods and applications of utilizing ant colony optimization algorithms. New methods and theory such as multi colony ant algorithm based upon a new pheromone arithmetic crossover and a repulsive operator, new findings on ant colony convergence, and a diversity of engineering and science applications from transportation, water resources, electrical and computer science disciplines are presented.

How to reference

In order to correctly reference this scholarly work, feel free to copy and paste the following:

Eva Rajo-Iglesias, Óscar Quevedo-Teruel and Luis Inclán-Sánchez (2011). On the Use of ACO Algorithm for Electromagnetic Designs, Ant Colony Optimization - Methods and Applications, Avi Ostfeld (Ed.), ISBN: 978-953-307-157-2, InTech, Available from: http://www.intechopen.com/books/ant-colony-optimization-methods-and-applications/on-the-use-of-aco-algorithm-for-electromagnetic-designs

INTECH
open science | open minds

InTech Europe
University Campus STeP Ri
Slavka Krautzeka 83/A
51000 Rijeka, Croatia
Phone: +385 (51) 770 447
Fax: +385 (51) 686 166
www.intechopen.com

InTech China
Unit 405, Office Block, Hotel Equatorial Shanghai
No.65, Yan An Road (West), Shanghai, 200040, China
中国上海市延安西路65号上海国际贵都大饭店办公楼405单元
Phone: +86-21-62489820
Fax: +86-21-62489821

© 2011 The Author(s). Licensee IntechOpen. This chapter is distributed under the terms of the Creative Commons Attribution-NonCommercial-ShareAlike-3.0 License, which permits use, distribution and reproduction for non-commercial purposes, provided the original is properly cited and derivative works building on this content are distributed under the same license.

IntechOpen

IntechOpen